RSC Advances

N-doped ordered mesoporous carbon (N-OMC) grafted on activated carbon fibers (ACF) composites (ACF@N-OMC) with enhanced activity for the electro-Fenton degradation of brilliant red X3B

Journal:	*RSC Advances*
Manuscript ID:	RA-ART-10-2014-011930.R1
Article Type:	Paper
Date Submitted by the Author:	29-Oct-2014

Complete List of Authors:	Peng, Qiaoli; South-Central University for Nationalities, key Laboratory of Catalysis and Material Sciences of the State Ethnic Affairs Commission & Ministry of Education Zhang, Zehui; South-Central University for Nationalities, key Laboratory of Catalysis and Material Sciences of the State Ethnic Affairs Commission & Ministry of Education Huang, Zi'ai; South-Central University for Nationalities, key Laboratory of Catalysis and Material Sciences of the State Ethnic Affairs Commission & Ministry of Education Ren, Wei; South-Central University for Nationalities, key Laboratory of Catalysis and Material Sciences of the State Ethnic Affairs Commission & Ministry of Education Sun, Jie; South-Central University for Nationalities, key Laboratory of Catalysis and Material Sciences of the State Ethnic Affairs Commission & Ministry of Education

Cite this: DOI: 10.1039/c0xx00000x

www.rsc.org/xxxxxx

ARTICLE TYPE

N-doped ordered mesoporous carbon (N-OMC) grafted on activated carbon fibers (ACF) composites (ACF@N-OMC) with enhanced activity for the electro-Fenton degradation of brilliant red X3B

Qiaoli Peng, Zehui Zhang*, Ze'ai Huang, Wei Ren, Jie Sun*

Received (in XXX, XXX) Xth XXXXXXXXX 20XX, Accepted Xth XXXXXXXXX 20XX
DOI: 10.1039/b000000x

N-doped ordered mesoporous carbon (N-OMC) was successfully prepared using dicyandiamide ($C_2H_4N_4$) as nitrogen source, and it was grafted on activated carbon fibers (ACF) to form carbon composites (abbreviated as ACF@N-OMC). The resultant ACF@N-OMC materials were used as cathode for the electro-Fenton degradation of organic pollutants using brilliant red X3B as molecular probe. Compared with the nitrogen free carbon materials, our prepared ACF@N-OMC materials showed higher electrocatalytic activity. On the one hand, the doped nitrogen ACF@N-OMC cathode materials reduced overpotential of O_2 reduction in the cathode. On the other hand, the introduction of nitrogen in ACF@N-OMC had larger pore size, which was beneficial the O_2 diffusion to produce much more reactive species. It is worth noting that the electrocatalytic activity of ACF@N-OMC cathode materials depends on the nitrogen content. With the increase of the nitrogen content, its activity firstly increased, and then it deceased. In addition, ACF@N-OMC materials were stable and could be reused for at least 6 times in the E-Fenton degradation of X3B without the significant loss of its activity.

1. Introduction

With the development of chemical industry, persistent organic pollutants such as dyes, pesticides, and plasticizers have caused seriously environmental issues due to their direct discharge in aqueous effluent. Therefore, efficient removal of organic pollutants from wastewater has become a hot research topic in current. Nowadays, several different technological methods are available for the treatment of persistent organic pollutants such as bioremediation and physical adsorption. [1, 2]

Nowadays, advanced oxidation processes (AOPs) are technologies with significant importance in environmental restoration applications, which involves the generation of highly reactive oxidizing species able to attack and degrade organic substances. [3, 4] Among them, electro-Fenton (E-Fenton) reaction has proven to be one of the most effective methods to degrade organic pollutants in wastewater.[5] This technology is based on the *in situ* generation of H_2O_2, which generates highly reactive species such as hydroxyl radical in the presence of Fe^{2+} to degrade organic pollutant. On the meanwhile, the formed Fe^{3+} is then reduced to Fe^{2+} by organic intermediate radicals to complete a cycle.

Considering the fact that H_2O_2 is not stable and costly for transportation, E-Fenton systems have recently been attracted considerable attention, as H_2O_2 can be generated in-situ by the reduction of O_2 on the surface of cathode material. The E-Fenton system mainly includes four steps. Firstly, molecular oxygen in aqueous solution nearby cathode is reduced to H_2O_2 in an acidic solution [Eq. (1)]. Then, H_2O_2 formed on the surface of cathode diffuses into the solution and reacts with Fe^{2+} to generate •OH radicals [eq. (2)], which are reactive oxygen species in the degradation of organic pollutants [Eq. (3)]. On the meanwhile, Fe^{3+} is reduced to Fe^{2+} [Eq. (4)].

$$O_2 + 2H^+ + 2e^- \rightarrow H_2O_2 \quad (1)$$

$$Fe^{2+} + H_2O_2 + H^+ \rightarrow Fe^{3+} + H_2O + \bullet OH \quad (2)$$

$$\bullet OH + RH \rightarrow R\bullet + H_2O \quad (3)$$

$$Fe^{3+} + e^- \rightarrow Fe^{2+} \quad (4)$$

Q. L. Peng, Prof. Z. H. Zhang, Z. Huang, W. Ren and Prof. J. Sun
Department of Chemistry, Key Laboratory of Catalysis and Material Sciences of the State Ethnic Affairs Commission & Ministry of Education.
South-Central University for Nationalities
MinYuan Road 708, Wuhan, R.P. China
Fax: (+)86-27-67842752
E-mail: zhangzehui@mail.ustc.cn& jetsun@ mail.scuec.edu.cn

Compared with traditional Fenton method, E-Fenton is eco-friendly methods that have recently received much attention for water remediation. Compared to the conventional Fenton process, the electro-Fenton process has the advantage of allowing better control of the process and avoiding the storing and transport of the H_2O_2.[6] Over the past decade, the cathode materials used in E-Fenton system mainly focused on carbonaceous materials such as graphite,[7] activated carbon,[8, 9] carbon nanotubes,[10] activated carbon fibers (ACF) and even PTFE-carbon felt,[11] as these carbonaceous materials show good conductivity, stability, high surface area and chemical resistance.[12, 13] In order to improve the efficiency of E-Fenton system, it is important to develop new cathode material with high ability to generate H_2O_2 by the reduction of oxygen. As a new kind of carbon materials, ordered mesoporous carbon (OMC) shows some excellent advantages high surface area, tunable pore size, interconnected pore network, and tailorable surface properties, and it has been widely used in catalysis,[14] electro-absorption, supercapacitor,[15] hydrogen storage[16] and capacitive deionization.[17] Recently, OMC has been attracted much attention in electrochemical reaction.[18, 19] Very recently, our group successfully prepared a new kind of oxygen-fed gas diffusion cathode composites (ACF covered by OMC), by the coat of OMC on the surface of ACF (ACF@OMC), which showed excellent efficiency in E-Fenton degradation of organic dye.[20] However, it still has the room to improve the concentration of H_2O_2 generated in-situ by the reduction of oxygen on surface of the cathode. Additionally, the previous E-Fenton system required high voltage (6.2V) due to the high overpotential. From the viewpoint of economy, the development of new cathode materials with low overpotential is of great importance.

It has been shown that nitrogen doping of carbon materials can enhance the surface properties, namely surface polarity, electric conductivity, and electron-donor affinity, which has been used in many fields such as CO_2 capture,[21] electric double-layer capacitors,[22] fuel cells,[23] and catalysis.[24] Inspired by the advantages of N-doped carbon materials, the aim of this present study was to develop a new kind of N-doped OMC, which was then coated with a layer of ACF to construct core-shell ACF@N-OMC cathode material, and used for the E- Fenton degradation of X3B.

2. Experimental Section

2.1. Materials

All chemicals were supplied by Sinopharm Co. Ltd. (Shanghai, China). Copolymer Pluronic F127 ($EO_{106}PO_{70}EO_{106}$) was purchased from Sigma. ACF was purchased from Xuesheng Technology (Shandong, China), and Brilliant red X3B dye was purchased from Jining dye manufacture (Jinlin, China). All chemicals were used directly without purification, and all aqueous solutions were prepared with ultrapure water (>18 MΩ·cm) obtained from Millipore system.

2.2 Preparation of the ACF@N- OMC cathode materials

ACF (3.0 cm × 3.0 cm) was firstly calcined at 800 °C under nitrogen atmosphere for 6 h before use. N-OMC was prepared by a soft-template method using copolymer F127 as a template,[25] and ACF@N-OMC was prepared by surface coating method. Typically, F127 (1.0 g) and certain amounts of dicyandiamide (0-2.5 g) were firstly dissolved in a mixture of ethanol (20 g) and water (10 g). Then, 5.0 g of resol ethanol solution (20 wt %), which was prepared according to literature,[26] was added and stirred for 0.5 h. The resultant homogeneous solution was then poured into a dish which was filled with 1.0 g of ACF, and the mixture in the dish was kept still for 8 h at room temperature. Then the dish was heated in an oven at 100 °C for 24 h to evaporate the solvent. ACF@N-OMC cathode materials heterogeneity were obtained by separation of the formed ACF-gel composite from the dish, and followed by calcination at 250 ℃ for 2 h and then 600 ℃ for 3 h with a ramp rate of 1 ℃·min^{-1} under N_2 atmosphere. The prepared ACF@N-OMC samples were denoted as Sx (Table 1), where x is the mass weight of dicyandiamide (g).

2.3 Characterization

The morphology of the carbonous cathode material was observed on a field emission scanning electron microscope (SEM) (Hitach, Japan) with an acceleration voltage of 20 kV. The pore structures of N-OMC, which was dropped from the surface ACF@N-OMC composites after ground, was observed by a transmission electron microscopy (TEM) (Tecnai G20, USA) using an acceleration voltage of 200 kV. Nitrogen sorption isotherms were measured with an Autosorb-1 (Quantachrome, USA) at 77 K. Prior to the measurement, all the samples were degassed at 200 °C for 6 h in a vacuum line. The BET surface area was determined by a multipoint BET method using the adsorption data in the relative pressure (P/P_0) range of 0.05–0.3. The mesoporous pore size distributions were derived from desorption branches of isotherms by using BJH model. X-ray photoelectron spectroscopy (XPS) measurement was done using Multilab 2000 XPS system with a monochromatic Mg Kα source and a charge neutralizer, all the binding energies were referenced to the C 1s peak at 284.4 eV of the surface adventitious carbon.

2.4 Electrochemical Property Measurements

The electrochemical performance of the electrode was evaluated by cyclic voltammetry (CV) using an Electrochemical Station (CHI-650D, China), carried between -2.0 and +1.0 V at room temperature, the scan rate was 100 mV s^{-1}. The electrodes include as-prepared carbon electrode, Pt plate, and saturated calomel electrode (SCE), which were used as working electrode, counter electrode, and the reference electrode, respectively. 0.1 mol/L Na_2SO_4 solution (pH 3.0) was used as the electrolyte.

2.5 E-Fenton degradation

E-Fenton degradation was carried out in a 250 mL beaker containing 200 mL of solution and equipped with two electrodes under magnetic stir at room temperature. The cathode was assembled by attaching 1.0 g of the prepared ACF@N-OMC carbon materials in size of 3.0 cm×3.0 cm on the surface of Ti plate, and a piece of graphite paper (3.0 cm×3.0 cm) was used as anode. Before E-Fenton degradation, the solution containing 1.0×10^{-4} mol L^{-1} X3B, 0.1 mol L^{-1} Na_2SO_4 and 1.0×10^{-3} mol L^{-1} $(NH_4)_2Fe(SO_4)_2$•$7H_2O$ was adjusted to pH 3.0 by diluted H_2SO_4, and was kept stirring and bubbled with an oxygen flow rate of 0.6

$Lmin^{-1}$ for 5 h to establish the adsorption-desorption equilibrium of the dye. During E-Fenton degradation, the electric current on the electrode system was kept 30 mA by using CHI-650D (Shanghai, China) as the potentiostat, and the voltage between anode and cathode on the electrode system was kept at about 3.0 V. The prepared cathode was selected as working electrode, the graphite electrode was as counter electrode and saturated calomel electrode (SCE) was as reference electrode. The distance between the working electrode and counter electrode was 3 cm. At certain time intervals, small aliquots were withdrawn by a syringe, and filtered through a membrane (pore size of 0.45 μm). The concentration of X3B dye remaining in the filtrate was then analyzed by a UV1800 spectrometer (Shanghai, China) at 530 nm.

2.6 Detection of the formed H_2O_2.

The amount of H_2O_2 was detected by UV-Vis spectrophotometry based on the reported method.[27] The experimental conditions for the generation of H_2O_2 were almost the same with the E-Fenton degradation process without the addition of X3B and Fe^{2+}. At given intervals of reaction, 1.5 ml of filtrate was mixed with 0.75 ml of potassium biphthalate (0.1 mol L^{-1}), followed by the addition of 0.75 mL of iodide reagent which contains potassium iodide (0.4 mol L^{-1}), NaOH (0.06 mol L^{-1}) and ammonium molybdate (0.1 mmol L^{-1}). The mixture was kept still for 2 min, and then measured by UV-Vis spectrophotometry at 352 nm.

2.7 Measurement of •OH radicals.

The •OH radicals were determined by photoluminescence (PL) method using coumarin as molecular probe, which readily reacts with •OH to produce highly fluorescent product, 7-hydroxycoumarin.[28, 29] 200 mL of mixed solution containing coumarin (0.5 $mmolL^{-1}$), 0.1 $molL^{-1}$ Na_2SO_4 and 1.0 $mmolL^{-1}$ $(NH_4)_2Fe(SO_4)_2•7H_2O$, were adjusted to pH 3.0 by diluted H_2SO_4. The electrodes and the electric current were the same as mentioned in E-Fenton degradation process. The filter was analyzed on a Hitachi F-7000 fluorescence spectrophotometer by the excitation with the wavelength of 332 nm.

3. Results and Discussion

3.1 Characterization of ACF@N-OMC materials

The morphology of activated carbon fibers was hair-like structure with an average diameter of 10 μm as described in our previous work.[20] Fig. 1 shows the SEM images of the as-prepared ACF@N-OMC composites, the morphology of which was similar as that of ACF at first glance. However, careful view that ACF@N-OMC is not so smooth as pristine ACF, and the roughness of ACF@N-OMC increases with an increase in the amount of dopant (Fig. 1a-e). As shown in Fig. 1, ACF@N-OMC cathode materials are core-shell structured, as ACF was coated by a layer N-OMC. As The thickness of N-OMC lay is estimated to be 1 μm (Fig. 1f).

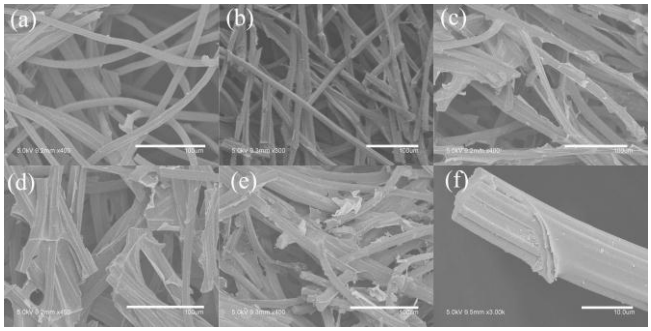

Fig.1. SEM images of S0(a), S0.5(b), S1.0(c), S1.5(d) and S2.5(e), respectively. The scale bars are 100μm. (f) is high-resolution SEM of S1.0 showing the core-shell structured ACF@N-OMC cathode materials. The scale bar is 10μm.

The pore structure of N-OMC layer, which was exfoliated from the surface of ACF@N-OMC composites by grinding, was further observed by TEM (Fig. 2). Fig. 2a-c show typically pore structure of N-OMC layer for S0, S0.5 and S1.0 sample, respectively. It is clearly seen that there are many stripes in parallel, reflecting their highly ordered mesoporous structures. High resolution TEM image for N-OMC layer of S1.0 sample shows that the pores are in an average diameter of 4 nm (Fig. 2f). The formed ordered mesoporous channels can facilitate the diffusion of air, and therefore improve the efficiency for the reduction of oxygen on the surface of ACF@N-OMC cathode materials (Eq. 1), which will be discussed below. However, the mesoporous structures become disordered when the amount of dopant beyond 1 g (Fig. 2d and e).[25] From the SEM and TEM images, it is confirm that N-OMC was successfully grafted on the surface of ACF.

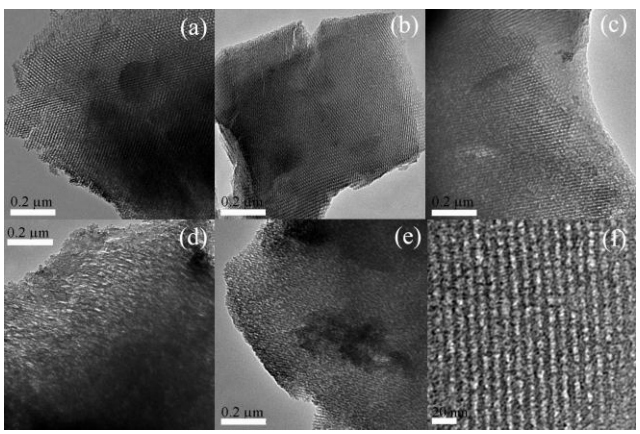

Fig.2. TEM images of S0(a), S0.5(b), S1.0(c), S1.5(d) and S2.5(e), respectively. The scale bars are 0.2μm. (f): the high-resolution TEM image showing the ordered mesopores of S1.0 sample. The scale bar is 20nm.

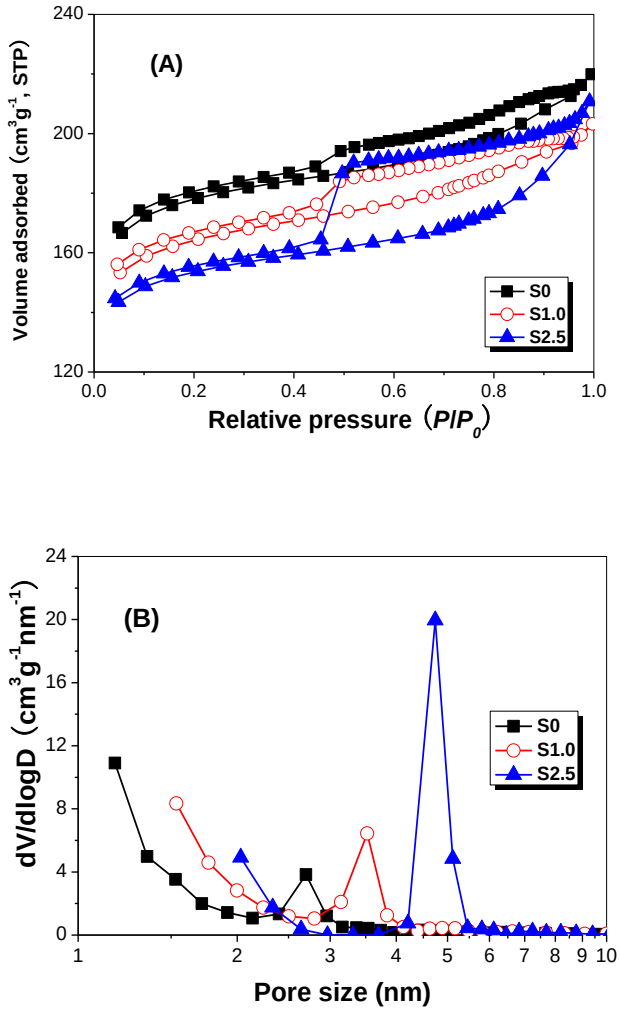

Fig. 3. Nitrogen sorption isotherms (A) and pore size distributions (B) of ACF@N-OMC samples.

Nitrogen adsorption measurements were further used to characterize the textile structure of ACF@N-OMC materials. Fig. 3A shows the nitrogen adsorption-desorption isotherms. All of the isotherms are type-IV with hysteresis loops (Type H1) in the relative pressure of 0.4–0.9.[30, 31] With the increase of nitrogen content, the adsorption isotherm shifts downward while the capillary condensation step shifts to high relative pressure. This phenomenon indicates that there is a decrease in BET surface areas and an increase in average pore size of ACF@N-OMC with the increase of nitrogen content, which matches well with the pore size distribution curves (Fig 3B). BET surface area of ACF@N-OMC was found to decrease from 534 to 440 m^2g^{-1}, and the pore size dramatically increases from 2.7 to 4.7 nm (Table 1) with the dosage of dicyandiamid from 0 to 2.5 g, which are consistent with the previous results.[32] However, too much dopant is not beneficial to the formation of ordered pore structures of N-OMC (Fig. 2). Pores with larger size are beneficial for oxygen diffusion and the following reduction of oxygen on ACF@N-OMC, while the decreased BET surface area will result in the reduction of active sites. Therefore, an optimum amount of dicyandiamide is expected to be existed in fabrication of the high efficient carbonous cathode materials.

Table 1. Physical properties of the prepared ACF@N-OMC samples.

Sample	Dicyandiamide (g)	S_{BET} (cm^2g^{-1})	PV (cm^3g^{-1})	APS (nm)
S0	0	538	0.36	2.7
S0.5	0.5	515	0.32	3.0
S1.0	1.0	501	0.35	3.5
S1.5	1.5	498	0.34	4.1
S2.5	2.5	440	0.33	4.7

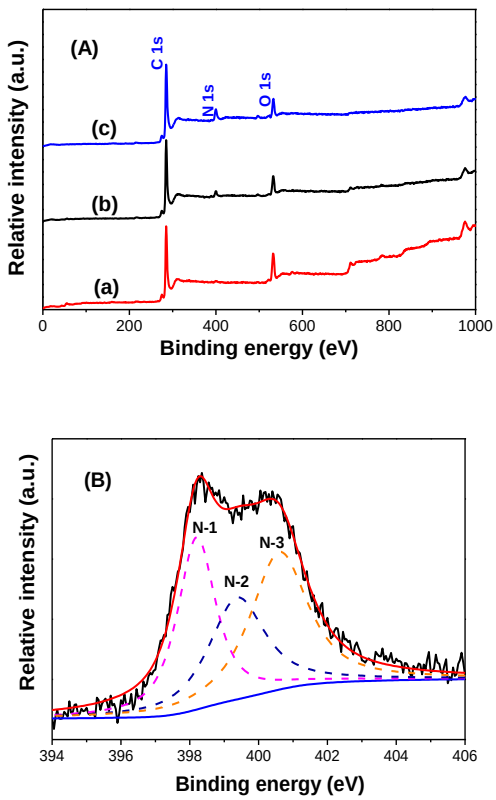

Fig. 4. XPS spectra of the samples. (A) The survey scan of S0(a), S1.0(b) and S2.5(c); (B) The N1S region.

X-ray photoelectron spectroscopy (XPS) technique was further employed to characterize the ACF@N-OMC materials. Fig. 4A shows XPS elemental survey scans of S0, S1.0 and S2.5 samples. For the nitrogen free sample S0, the survey spectrum only gives signals of C 1S and O 1S, indicating that S0 only contains C and O elements. However, three XPS peaks with C 1S, N 1S and O

1S are present in S1.0 and S2.5, which clearly indicates that the nitrogen has been successfully doped into ACF@N-OMC materials.[33, 34] Moreover, the intensity of N 1S was found to increasing with increase in the amount of dicyandiamide. According to the XPS element analysis, the contents of N element in S1.0 and S2.5 are detected to be 5.49, and 8.39 at.%, respectively.

To further evaluate the bonding configuration of N element in ACF@N-OMC composites, high resolution XPS spectra of N 1S region was also collected. As shown in Fig. 4(B), XPS spectrum of N 1s for S1.0 sample can be well deconvoluted into three peaks centered at 398.3, 399.7 and 400.7 eV, respectively. The three peaks are attributed to pyridinic N (N-1),[35] pyrrolic N (N-2),[36] and graphitic N (N-3),[37] respectively. There is no peak associated with nitrogen bonded to oxygen, which would appear at 404−408 eV, suggesting that the oxygen atoms in ACF@N-OMC cathode materials might be bonded to the carbon atoms .[38]

3.2. E-Fenton degradation

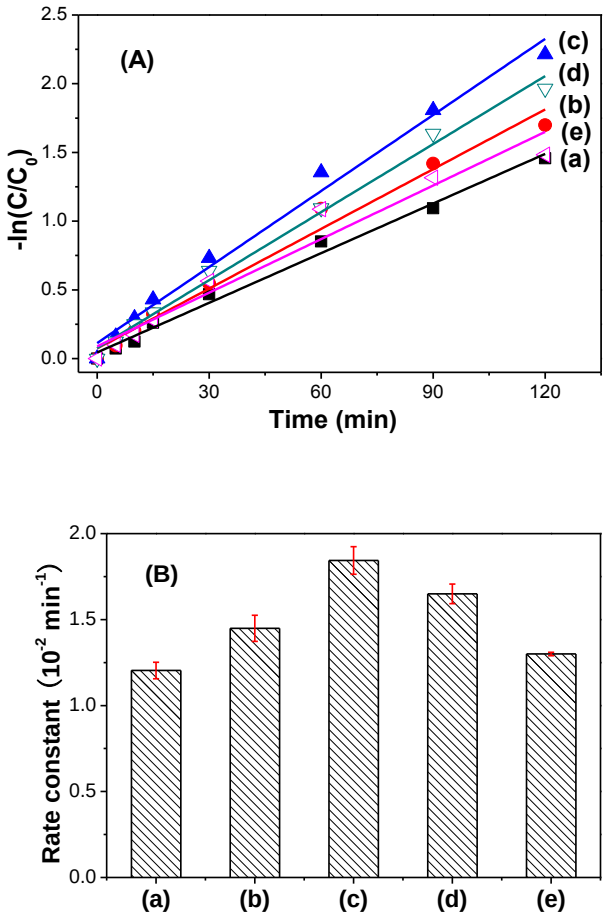

Fig. 5. Photocatalytic degradation kinetics (A) and comparison of the corresponding rate constants (B) of X3B degradation in Electro-Fenton system using ACF@N-OMC of S0(a), S0.5(b), S1.0(c), S1.5(d) and S2.5(e) as cathode materials, respectively. Conditions: pH 3.0, Na_2SO_4 0.1 M, Fe^{2+} 1 mM, initial X3B concentration 0.1m M, electric current 30 mA, air flow rate 0.6 $Lmin^{-1}$, T=25 °C.

The activity of ACF@N-OMC cathode materials was evaluated by the degradation of X3B dye in E-Fenton system. Fig. 5A shows E-Fenton degradation kinetics of X3B by the use of different ACF@N-OMC cathode materials. It is clearly seen that the degradation profiles of X3B obey pseudo-first-order reaction rate equation in kinetics. The degradation rate constant, an indicator of the activity of the cathode materials, increased firstly and then deceased with the increase of nitrogen content (Fig. 5B). S1.0 sample shows the highest reactivity with degradation rate of 1.84×10^{-2} min^{-1}, which is 50% higher than that of undoped sample S0 (rate constant of 1.20×10^{-2} min^{-1}). Although undoped S0 sample possesses the largest BET specific surface area (538 m^2g^{-1}) among all the prepared ACF@OMC cathode materials (Table 1), it shows the lowest reactivity in E-Fenton degradation of X3B dye (Fig. 5B). These results indicated nitrogen in ACF@OMC cathode materials played a positive role in the E-Fenton degradation of X3B, and the reasons are discussed as below. However, the catalytic activities of S1.5 and S2.5 were lower than that of S1.0.

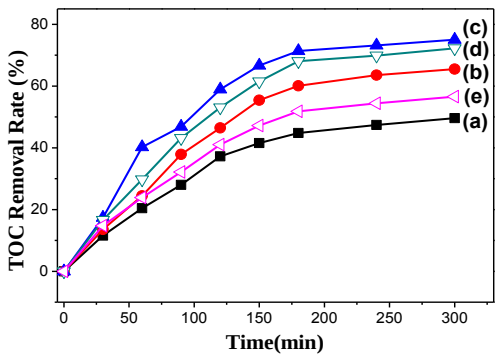

Fig. 6. Mineralization of X3B degradation in Electro-Fenton system using ACF@N-OMC of S0(a), S0.5(b), S1.0(c), S1.5(d) and S2.5(e) as cathode materials, respectively. Conditions: pH 3.0, Na_2SO_4 0.1 M, Fe^{2+} 1 mM, initial X3B concentration 0.1mM, electric current 30 mA, air flow rate 0.6 $Lmin^{-1}$, T=25 °C.

Mineralization of X3B solution in E-Fenton process was monitored by TOC loss. Fig. 6 shows the results of the TOC decay of X3B through E-Fenton reaction by the use of different ACF@N-OMC cathode materials. It is noted that the change tendency of the effect of ACF@N-OMC cathode materials on the mineralization of X3B is the same as that of the degradation kinetics. As shown in Fig. 6, the lowest mineralization of 49.6% was obtained 5 h of E-Fenton reaction when nitrogen free S0 was used as the cathode. S0 sample shows both the lowest degradation and mineralization ability of X3B. S1.0 sample not only shows the highest degradation kinetic but it also showed the highest mineralization ability with the TOC removal rate of 75% under the same conditions. According to the results from Fig. 5 and Fig. 6, it is clearly indicated that nitrogen plays a positive role in the E-Fenton degradation of X3B When using carbon materials as cathode. In addition, the content of nitrogen showed great effect on the texture on the cathode material, which further

affected the E-Fenton degradation ability of organic pollutants. Du et al., also reported the degradation of X3B by the Fenton reaction, in which about of 70% of X3B was degraded after 120 min.[39] Compared with the reported Fenton systmes, our reaction system is much more effective.

3.3 Cyclic voltammetry

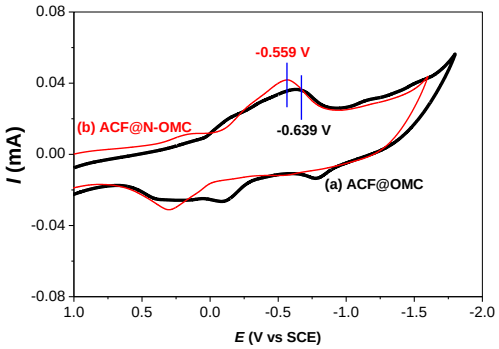

Fig. 7. Comparison of the cyclic voltammetry of ACF@OMC (a) and ACF@N-OMC (b) cathodes. Conditions: pH 3.0, Na_2SO_4 0.1 M, air flow rate 0.6 $Lmin^{-1}$, T=25 °C.

It is known that O_2 reduction on the surface of carbon electrode is an important process for electro-generation of H_2O_2 (Eq. 1). In order to understand the effect of N-doping on the overpotential of O_2 reduction on the surface ACF@N-OMC cathode materials, cyclic voltammetry experiments were carried out in 0.1 mol L^{-1} Na_2SO_4 aqueous solution at pH 3.0 (Fig. 7). A reduction peak at -0.639 V was observed for nitrogen free ACF@OMC cathode materials, which was attributed to the reduction peak of O_2. However, the reduction peak shifted to -0.559 V with an obviously enhanced current for N-doped S1.0 sample. These results indicate that nitrogen in the ACF@N-OMC reduced the overpotentials of O_2 reduction on the surface of cathode material, therefore, O_2 reduction is much easier after N-doping of ACF@OMC. Therefore, it is easily understandable that the as-prepared ACF@N-OMC showed enhanced E-Fenton reactivity in degradation of organic pollutants (Fig. 5 and 6).

3.4 Formation of H_2O_2 and measurement of •OH radicals.

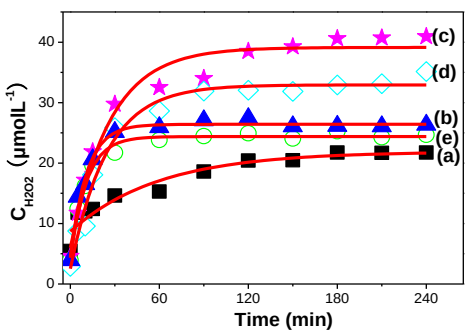

Fig. 8. Concentration of H_2O_2 detected as reaction time in E-Fenton system using S0(a), S0.5(b), S1.0(c), S1.5(d) and S2.5(e) as cathode materials, respectively. Conditions: pH 3.0, Na_2SO_4 0.1 M, electric current 30 mA, air flow rate 0.6 $Lmin^{-1}$, T=25 °C.

Since H_2O_2 is an important intermediate for the E-Fenton reaction (Eq. 1), the amount of H_2O_2 formed by the reduction of O_2 on the surface of ACF@N-OMC cathode materials was detected. The experiments were carried out in 0.1 mol L^{-1} of Na_2SO_4 solution at pH 3.0 in the absence of Fe^{2+} ions, and the voltage added between two electrodes was 3.0 V. As shown in Fig. 8, H_2O_2 was indeed produced during the E-Fenton process for all the prepared ACF@N-OMC cathode materials. It is noted that the concentration of accumulated H_2O_2 increased gradually and then reach a platform, which was consistent with the previous results reported by Wang *et al.*.[40] After reaction for about 1 h, the concentration of H_2O_2 reached a steady state. The fast increase in the concentration of H_2O_2 at beginning is due to the reduction of O_2 on the surface of ACF@N-OMC cathode materials. However, the formed H_2O_2 can also decompose into O_2 either on the anode (heterogeneous process) or in the medium (homogeneous process) even in the absence of Fe^{2+}.[41] When the formation rate is comparable to decomposition rate, the concentration of H_2O_2 will reach constant. After 2 h, the concentration of H_2O_2 in steady state with S1.0 as cathode material was measured to be 40.93 μmol L^{-1}, which is about 1.9 times higher than that using nitrogen free S0 sample as cathode material (21.75 μmol L^{-1}).

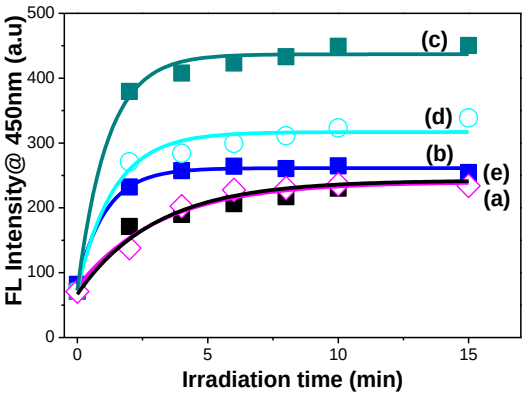

Fig. 9. Time dependence of the induced photoluminescence intensity @ 450 nm in E-Fenton system using S0(a), S0.5(b), S1.0(c, d), S1.5(e) and S2.5(f) as cathode materials, respectively. Conditions: pH 3.0, Na_2SO_4 0.1 M, Fe^{2+} 1 mM, coumarin concentration 0.5 mM, electric current 30 mA, air flow rate 0.6 $Lmin^{-1}$, T=25 °C.

To further confirm the formation of •OH in E-Fenton system (Eq. 2), coumarin is used as a probe to evaluate the formation of •OH radicals, which can readily react with •OH radicals to produce highly fluorescent product, 7-hydroxycoumarin.[27-28] It is observed that the photoluminescence intensity of the generated 7-hydroxycoumarin at 450 nm (excited at 332 nm) increases with reaction time at an early stage (Fig. 9). Then the photoluminescence intensity at 450 nm tends to a constant, which

has the same trend with that of the formation rate of H_2O_2 and X3B degradation. Therefore, it can be concluded that it is •OH radicals formed during E-Fenton reaction that are responsible for the degradation of the X3B dye (Eq. 2 and 3).

Compared with S1.0 cathode materials, the formation rate of H_2O_2 and •OH radicals in pristine S0 system is much slower (Fig. 8 and Fig. 9). Control experiment shows that little •OH radicals can be detected when S1.5 and S2.5 were used as cathode materials in E-Fenton system, reflecting the importance of ordered mesoporous structures of the carbonous cathode materials. The ordered mesopores can affect the electro-induced generation of H_2O_2 and •OH radicals that directly determine the ability of degradation of environmental pollutions in E-Fenton system (Eq. 1 and 2). In addition, hydroperoxyl radicals (•OOH) was also reported to be reactive oxidative species.[42]

3.5 Stability of ACF@N-OMC cathode materials.

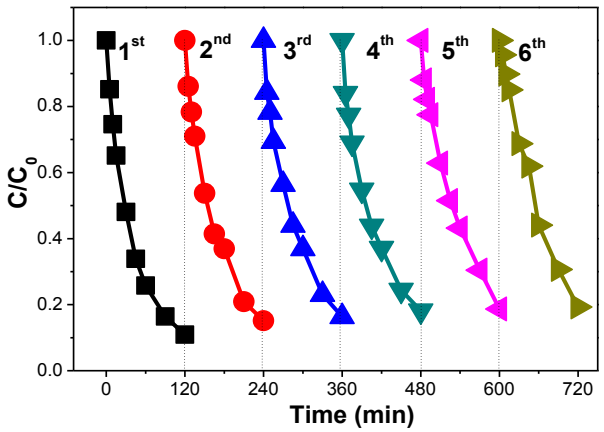

Fig. 10. Recycle experiments for E-Fenton degradation of X3B dye using S1.0 as cathode materials. Conditions: pH 3.0, Na_2SO_4 0.1 M, Fe^{2+} 1 mM, initial X3B concentration 0.1mM, electric current 30 mA, air flow rate 0.6 $Lmin^{-1}$, T=25 °C.

The recovery and reuse of the ACF@N-OMC cathode materials is one of the crucial step in determining the viability and overall efficiency of this potentially economic an environment-friendly process. Therefore the stability of the novel ACF@N-OMC cathode materials was evaluated using S1.0 as an example. 90.7% of the X3B dye was found to degrade when fresh S1.0 cathode material was used in the 1st run (within 120 min). Even after 6th run, the reactivity of S1 cathode materials almost keep unchanged after washing by water (Fig. 10), reflecting the promising usage of this novel carbonous cathode material in practical application.

4. Conclusions

In summary, N-doped ACF@N-OMC materials was successfully prepared and characterized. It can be used as cathode materials for the effective E-Fenton degradation of X3B. Compared with undoped counterpart, N-doped ACF@N-OMC cathode materials showed enhanced reactivity in E-Fenton degradation of X3B by a factor of 1.5. The enhanced reactivity of ACF@N-OMC is due to the decreased overpotential for O_2 reduction and enlarged mesopore size, which facilitate the diffusion and reduction of O_2. The novel cathode materials were stable, indicating its promising usage in practical application in many areas. This study may provide new insight into design and preparation of carbonous materials with superior efficiency.

Acknowledgements

This work was supported by the New Century Excellent Talents Foundation of China's Ministry of Education (NCET-13-1047), the National Natural Science Foundation of China (21477165) and Technology Centre Project of Wuhan City (2014060202010129).

References

1 X. M. Zhang, J. Y. Liu, S. J. Kelly, X. J. Huang, J.H. Liu, *J. Mater. Chem. A* 2004 **2**, 11759-11767

2 Z. H. Zhang, X.Y. Wen, K. J. Deng, B. G. Zhang, K. L. Lv, J. Sun, Catal. Sci. Technol. 2013, **3**, 1415-1422.

3 V. Vaiano, O. Sacco, D. Sannino, P. Ciambelli, S. Longo, V. Venditto, G. Guerra, J. Chem. Technol. Biotechnol. 2014, **89**, 1175-1181.

4 H. Q. Sun, C. Kwan, A. Suvorova, H. M. Ang, M. O. Tade, S. B. Wang, Appl. Catal. B:Environ. 2014, **154**, 134-141.

5 C. Jiang, S. Pang, F. Ouyang, J. Ma, J. Jiang, J. Hazard. Mater. 2010, **174**, 813–817.

6 P. V. Nidheesh, R. Gandhimathi, Desalination 2012, **299**, 1–15.

7 E. Brillas, I. Sirés, M. A. Oturan, Chem. Rev. 2009, **109**, 6570–6631.

8 C. C. Gilmour, G. S. Riedel, G. Riedel, S. Kwon, R. Landis, S. S. Brown, A. M. Charles, U. Ghosh, Environ. Sci. Technol. 2013, **47**, 13001-13010.

9 K. Cruz-González, O. Torres-López, A. García-León, J.L. Guzmán-Mar, L.H. Reyes, A. Hernández-Ramírez, J.M. Peralta-Hernández, Chem. Eng. J. 2010, **160**, 199–206.

10 Z. Ai, T. Mei, J. Liu, J. Li, F. Jia, L. Zhang, J. Qiu, J. Phys. Chem. C 2007, **111**, 14799-14803

11 A. R. Khataee, M. Zarei, L. Moradkhannejhad, Desalination 2010, **258**, 112–119.

12 E. Isarain-Chávez, C. Arias, P. L. Cabot, F. Centellas, R. M. Rodríguez, J. A. Garrido , E. Brillas, Appl. Catal. B: Environ. 2010, **96**, 361–369.

13 M. D. de Luna, M. L. Veciana, C. C. Su, M. C. Lu, J. Hazard. Mater. 2012, **217**, 200–210.

14 R. Liu, X. Q. Wang, X. Zhao, P. Y. Feng, Carbon 2008, **46**, 1664–1669.

15 H. J. Liu, X. M. Wang, W. J. Cui, Y. Q. Dou, D. Y. Zhao, Y. Y. Xia, J. Mater. Chem. 2010, **20**, 4223–4230.

16 L. Li, X.D. Yao, C. H. Sun, A. J. Du, L. N. Cheng, Z. H. Zhu, C. Z. Yu, J. Zou, S. C. Smith, P. Wang, H. M. Cheng, R. L. Frost, G. Q. Lu, Adv. Funct. Mater. 2009, **19**, 265-271.

17 L. Li, L. Zou, H. Song, G. Morris, Carbon 2009, **47**, 775–781.

18 C. F. Xue, Y. Y. Lv, F. Zhang, L. M. Wu, D. Y. Zhao, J. Mater. Chem. 2012, **22**, 1547-1555.
19 J. Zhi, S. Deng, Y. Zhang, Y. Wang, A. Hu, J. Mater. Chem. A 2013, **1**, 3171-3176.
20 J. J. Hu, J. Sun, J. K. Yan, K. L. Lv, C. Zhong, K. J. Deng, J. L. Li, Electrochem. Commun. 2013, **28**, 67–70.
21 G. P. Hao, W. C. Li, D. Qian, A.H. Lu, Adv. Mater. 2010, **22**, 853-857.
22 W. Xing, S. Z. Qiao, R. G. Ding, F. Li, G. Q. Lu, Z. F. Yan, H.M. Carbon 2006, **44** 216–224.
23 S. H. Joo, C. Pak, D. J. You, S. A. Lee, H. I. Lee, J. M. Kim, H. Chang, D. Seung, Electrochim. Acta 2006, **52**, 1618-1626.
24 P. Krawiec, E. Kockrick, L. Borchardt, D. Geiger, A. Corma, S. Kaskel, J. Phys. Chem. C 2009, **113**, 7755–7761.
25 J. Wei, D. Zhou, Z. Sun, Y. Deng, Y. Xia, D. Zhao. Adv. Funct. Mater. 2013, **23** 2322–2328.
26 Y. Meng, D. Gu, F. Q. Zhang, Y. F. Shi, L. Cheng, D. Feng, Z.X. Wu, Z. X. Chen, Y. Wan, A. Stein, D. Y. Zhao, Chem. Mater. 2006, **18**, 4447–4464.
27 C. Kormann, D.W. Bahnemann. Environ. Sci. Technol. 1988, **22**, 798-806.
28 Z. H. Zhang, M. J. Zhang, J. Deng, K. J. Deng, B. G. Zhang, K. L. Lv, J. Sun, L. Q. Chen, *Appl. Catal. B* : Envrion. 2013, **132-133**, 90-97.
29 Z. H. Zhang, Q. L. Peng, J. Sun, L. P. Fang, K. J. Deng, *Ind. Eng. Chem .Res.* 2013, **52**, 13342–13349.
30 Y. Meng, D. Gu, F. Zhang, Y. Shi, H. Yang, Z. Li, C. Z. Yu, B. Tu, D. Y. Zhao, Angew. Chem. Int. Ed. 2005, **44**, 7053–7059.
31 M. Ignat, C.J. Van Oers, J. Vernimmen, M. Mertens, S. Potgieter-Vermaak, V. Meynen, E. Popovici , P. Cool, Carbon 2010, **48**, 1609–1618.
32 G. Y. Xu, B. Ding, P. Nie, L. F. Shen, J. Wang, X. G. Zhang, Chem.-Eur. J. 2013, **19**, 12306-12312.
33 S. S. Feng, W. Li, Q. Shi, Y.H. Li, J. C. Chen, Y. Ling, A. M. Asiri, D. Y. Zhao, Chem. Commun. 2014, **50**, 329-331.
34 J. Liang, X. Du, C. Gibson, X. W. Du, S. Z. Qiao, Adv. Mater. 2013, **25**, 6226–6231.
35 H. C. Chen, F. G. Sun, J.T. Wang, W. C. Li, W. M. Qiao, L. C. Ling, D. H. Long, J. Phys. Chem. C 2013,**117**, 8318–8328.
36 U. B. Nasini, V. G. Bairi, S. K. Ramasahayam, S. E. Bourdo, T. Viswanathan, A. U Shaikh, J. Power Sources 2014, **250**, 257-265.
37 X. Y. Chen, C. Chen, Z. J. Zhang, D. H. Xie, J. Mater. Chem. A 2013, **1**,10903-10911.
38 G. Wang, S. Kuang, D. Wang, S. Zhuo, Electrochim. Acta 2013, **113**, 346–353.
39 W. P. Du, Q. Sun, X. J. Lv, Y. M. Xu, Catal. Commu. 2009, 10, 1854-1858.
40 A. Wang, Y. You-Li, A. L. Estrada, Appl. Catal. B: Environ. 2011, **102**, 378–386.
41 A. Dirany, I. Sirés, N. Oturan, A. Özcan, M. A. Oturan, Environ. Sci. Technol. 2012, **46**, 4074–4082.
42 Y. Fan, Z.H. Ai, L.Z. Zhang, J. Hazard. Mater. 2010, **176**, 678-684.

